Threshold effects in light scattering from a binary diffraction grating

B. B. Anderson, A. M. Brodsky, and L. W. Burgess
Department of Chemistry, Center for Process Analytical Chemistry, University of Washington, Seattle, Washington 98195
(Received 15 January 1996)

The theory of light scattering from an interface covered by a periodic grating near the threshold of transformation of one of the diffraction beams from a traveling wave to an evanescent one is developed and compared with experiments. It is shown that the behavior of the scattered light near such thresholds provides rich information regarding both the medium in contact with the grating interface and the interface itself. [S1063-651X(96)11107-7]

PACS number(s): 42.25.−p

I. INTRODUCTION

Recent advances in the fabrication of high-quality diffraction gratings on dielectric substrates with periods of the order of the wavelength of visible light [1] have stimulated their use for spectroscopic studies of surfaces and properties of media separated by the grating covered interface [2,3]. Sainov and co-workers, using a relatively old idea first proposed by Rytov and Fabelynskii [4], have constructed a binary metal grating device on glass, working in total internal reflection mode, as a sensor for the determination of absorbance in liquid samples. In our work [5] we have demonstrated the wide possibilities for spectroscopic monitoring of static and dynamic properties of media near grating covered boundaries by analyzing the light scattering near the thresholds of the transformation of one of the transmitted diffracted beams from a traveling wave to an evanescent one. This monitoring method is termed grating light reflection spectroscopy (GLRS).

The applications of GLRS demands the development of an adequate theoretical interpretation of the corresponding effects of light reflection from gratings. The existing theories of grating light scattering [6,7] are based mainly on perturbation theory in the parameter l/λ, where l is the height of the grating and λ is the wavelength of incident light. Such perturbation approaches cannot be used in the interpretation of the singular behavior of the diffracted transmitted or reflected light in the parameter intervals near the thresholds of the transformation of one of the diffracting beams from a traveling wave to an evanescent one.

In this paper, we develop and compare with experiments the nonperturbative theory of GLRS, which allows us to establish the connections between the reflection amplitudes and phases for different diffraction channels. The theory is analogous to, with some modifications, the general threshold theory of multichannel wave scattering [8,9]. It is shown that analysis of the threshold behavior in light scattering allows us to obtain information about the complex dielectric function of the sample in contact with the grating as well as information regarding the interface and the grating itself. The scope of the information increases in the cases where it is possible to combine the perturbation theory of light scattering in individual diffraction channels with the general threshold theory.

This paper is organized as follows. In Sec. II, we describe the threshold theory of GLRS. The experimental procedures and techniques are described in Sec. III. In Sec. IV, we present the experimental results and the comparison of theory with experiments. In conclusion, we will summarize the results and discuss possible applications of GLRS.

II. THEORY

We consider in this section the threshold theory of light scattering (reflection and transmission) at a plane interface between substrate and analyte media containing a periodic grating layer with period Λ of the order of the wavelength of incident light (see Fig. 1). For simplicity we illustrate the method of calculation on an example of the system described by a local dielectric function $\varepsilon_{ij}(\overline{x})$ of the following form:

$$\varepsilon_{ij}(\overline{x}) = \varepsilon_0(x_1,\omega)\,\delta_{ij} + \delta\varepsilon_{ij}(\overline{x},\omega), \tag{1}$$

where $\varepsilon_0(x_1,\omega)$ describes the dielectric function averaged in the directions parallel to the surface and the interface component $\delta\varepsilon_{ij}(\overline{x},\omega)$ is periodic in the direction parallel to the surface:

$$\delta\varepsilon_{ij}(\overline{x},\omega) = \sum_{\substack{n=-\infty \\ n\neq 0}}^{\infty} \delta\tilde{\varepsilon}_{ij}(x_1,n,\omega)\, e^{in(\overline{q}\cdot\overline{x}_{\parallel})};$$
$$\overline{q} = \frac{2\pi}{\Lambda}\,\overline{g}, \quad \overline{x}_{\parallel} = \{x_2, x_3\}, \tag{2}$$

where $\overline{g}$ is the unit two-dimensional vector in the direction of the grating periodicity. We suppose that the thickness of the substrate-sample interface, l, is much less than the wavelength λ of the scattered light and

$$\delta\varepsilon_{ij}(\overline{x},\omega) = 0 \quad \text{for } |x_1| > l \ll \frac{c}{\omega} = \frac{\lambda}{2\pi}. \tag{3}$$

This inequality will allow us to estimate the coefficients entering into the general threshold approximation with the relative accuracy on the order of

$$O\left(\frac{l}{\lambda}\right)^2. \tag{4}$$

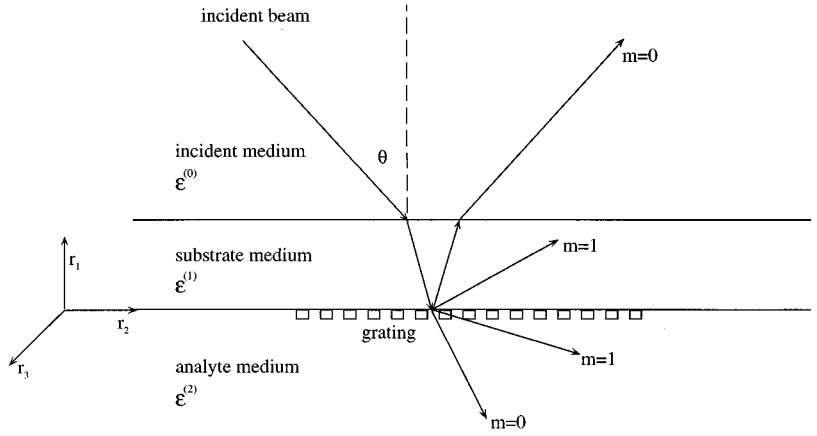

FIG. 1. The experimental scheme and ray trace diagram of the GLRS threshold phenomenon. The $m=0$ and $m=1$ diffraction orders only are shown here for simplicity.

Beyond the interface interval separating the substrate (1) and sample (2) media the dielectric function is supposed to be equal to frequency-dependent bulk values:

$$\varepsilon_0(x_1,\omega)=\begin{cases}\varepsilon^{(1)}(\omega) & \text{for } x_1>l \text{ for substrate medium}\\ \varepsilon^{(2)}(\omega) & \text{for } x_1<-l \text{ for sample medium.}\end{cases} \tag{5}$$

The distance of the air-substrate interface from the sample in the experimental device (see Fig. 1) is supposed to be much larger than the free space wavelength. This allows us to concentrate on the analysis of the light scattering at the substrate-sample interface. Note that the results of the calculations in the threshold approximation are very general in nature and can be generalized to the more complex cases, i.e., when the dielectric function is nonlocal.

We suppose that the imaginary part of $\varepsilon^{(1)}=\varepsilon^{(1)}(\omega)$ can be neglected and the imaginary part of $\varepsilon^{(2)}=\varepsilon^{(2)}(\omega)$ is relatively small:

$$\begin{aligned}&\mathrm{Im}\varepsilon^{(1)}\cong 0,\\ &\mathrm{Im}\varepsilon^{(2)}\ll \mathrm{Re}\ \varepsilon^{(2)}.\end{aligned} \tag{6}$$

There exist the following basic sets of solutions (7a) and (7b) to Maxwell's equations with frequency ω in the infinite media with dielectric constants $\varepsilon^{(1)}$ and $\varepsilon^{(2)}$, correspondingly:

$$\begin{aligned}\overline{E_1^s}(\pm,\overline{k_\parallel})&=\frac{\sqrt{4\pi\omega}}{c}\,\frac{(\overline{k_\parallel}\times\overline{n_1})}{\sqrt{k_\parallel^2\cdot k_1^{(1)}}}\,e^{i(-\overline{k_\parallel}\cdot\overline{x_\parallel}\mp k_1^{(1)}x_1)},\\ \overline{E_1^p}(\pm,\overline{k_\parallel})&=\frac{\sqrt{4\pi\omega}}{c}\,\frac{[(\overline{k_\parallel}\times\overline{n_1})\times\overline{k^{(1)}}]e^{i(-\overline{k_\parallel}\cdot\overline{x_\parallel}\mp k_1^{(1)}x_1)}}{\sqrt{(\omega^2/c^2)\varepsilon^{(1)}k_\parallel^2\cdot k_1^{(1)}}},\end{aligned} \tag{7a}$$

$$\begin{aligned}\overline{E_2^s}(\pm,\overline{k_\parallel})&=\frac{\sqrt{4\pi\omega}}{c}\,\frac{(\overline{k_\parallel}\times\overline{n_1})}{\sqrt{k_\parallel^2\cdot k_1^{(2)}}}\,e^{i(-\overline{k_\parallel}\cdot\overline{x_\parallel}\pm k_1^{(2)}x_1)},\\ \overline{E_2^p}(\pm,\overline{k_\parallel})&=\frac{\sqrt{4\pi\omega}}{c}\,\frac{[(\overline{k_\parallel}\times\overline{n_1})\times\overline{k^{(2)}}]e^{i(-\overline{k_\parallel}\cdot\overline{x_\parallel}\pm k_1^{(2)}x_1)}}{\sqrt{(\omega^2/c^2)\varepsilon^{(2)}k_\parallel^2\cdot k_1^{(2)}}},\end{aligned} \tag{7b}$$

where n_1 is the unit vector in the normal direction to the surface and

$$\overline{k^{1,2}}=\{k_1^{1,2},\overline{k_\parallel}\}, \tag{8}$$

$$\overline{k_\parallel}=\{k_2,k_3\},$$

$$k_1^{(1,2)}=\sqrt{(\omega^2/c^2)\varepsilon^{(1,2)}-k_\parallel^2}\equiv\frac{\omega}{c}\,\sqrt{\delta^{(1,2)}(k_\parallel)+i\ \mathrm{Im}\ \varepsilon^{(1,2)}},$$

$$\delta^{(1,2)}(k_\parallel)=\mathrm{Re}(\varepsilon^{(1,2)})-\frac{k_\parallel^2c^2}{\omega^2}.$$

The sign index $(+,-)$ in (7) corresponds to the direction of the wave toward and from the interface, respectively (incident and outgoing directions). Note the different order of the signs in the exponents in expressions (7a) and (7b). The normalization in (7) is chosen in such a way that the component of Poynting's vector $S_1=S\cdot\overline{n_1}$ in the direction normal to the interface constructed from the solutions in (7) is equal to unity for real k_1.

The two-dimensional wave vector $\overline{k_\parallel}$ in the discussed scattering problem is always real. According to momentum conservation laws, only the following values of $k_\parallel$ in scattered and transmitted waves are possible:

$$\overline{k_{\parallel,m}}=\overline{k_\parallel^0}+m\overline{q},\quad m=0,\pm1,\pm2,\ldots, \tag{9}$$

where $\overline{k_\parallel^0}$ is the value of the tangential component of the wave vector in the incident light.

The normal component of the wave vector $k_1^{(2)}$ always has, according to Eq. (8), at least a small imaginary component due to the contribution of Im $\varepsilon^{(2)}$. Large imaginary components of $k_1^{(1,2)}$ correspond to values of $(k_{\parallel,m}^{(1,2)})^2$, which are larger than $(\omega^2/c^2)\varepsilon^{(1)}$ or $(\omega^2/c^2)\varepsilon^{(2)}$, when

$$\delta_m^{(i)}=\mathrm{Re}\varepsilon^{(i)}-(k_{\parallel,m})^2\,\frac{c^2}{\omega^2}<0\quad\text{for } i=1 \text{ or } 2. \tag{10}$$

The condition (10) corresponds to the possibility of the formation of evanescent waves in the systems with nonhomogeneous interfaces.

In the following we will refer to the members of the solution set (7) as channels and designate them, taking into account (9), as $E_\alpha^\pm$ with a combined index subscript α:

$$\alpha=\{i_\alpha,\zeta_a,m_\alpha\},$$
$$i_\alpha=1,2;\quad \zeta_\alpha=s,p;\quad m_\alpha=0,\pm1,\pm2,\ldots \tag{11}$$

and superscript $\pm$ corresponding to incident and outgoing directions, respectively.

The full solutions $E_\alpha^{(+)}(\overline{x})$ of the light scattering problem with the incident wave in the α channel can be represented beyond the interface region in the sample and substrate media in the following form:

$$E_\alpha^{(+)}(\overline{x})=\overline{E_\alpha^{+}}(\overline{x})+\sum_{\alpha'} r_{\alpha',\alpha}\overline{E_{\alpha'}^{-}}(\overline{x}) \quad \text{for } x_1^2>l^2, \tag{12}$$

where the term with an incident wave is present only at $x_1>l$ or $x_1<-l$ depending on the value of i_α and the set $E_{\alpha'}^{-}(\overline{x})$ includes outgoing and evanescent waves in the medium $i_{\alpha'}$. For simplicity we have excluded in (12) a contribution under the sum over α' from possible surface and longitudinal bulk waves. The generalization corresponding to the introduction of such waves is a straightforward one. The $\hat{\mathbf{r}}$ matrix, with the elements $r_{\alpha',\alpha}$, contains all scattering information. These elements $r_{\alpha',\alpha}$ obey the following relations due to time inversion symmetry:

$$r_{\alpha,\alpha'}(\varepsilon)=r^*_{\alpha',\alpha}(\varepsilon^*), \tag{13}$$

In addition to the set of solutions in (12) there is another set of solutions,

$$E_\alpha^{(-)}(\overline{x})=[E_\alpha^{(+)}(\overline{x})]^*|_{\overline{k}_\parallel\to-\overline{k}_\parallel,\varepsilon\to\varepsilon^*}, \tag{12'}$$

where the incoming and outgoing waves have been interchanged relative to the set $E_\alpha^{(+)}(\overline{x})$.

According to (8), (9), and (10), there are critical values of $\alpha=\alpha_{\rm cr}$ (threshold singularities) at which one of the transmitted or scattered waves transforms from a traveling wave (with possible attenuation due to absorption) to an evanescent wave. Such values of α are determined by the following condition:

$$\delta_{\alpha_{\rm cr}}=0. \tag{14}$$

Near the threshold (14) the behavior of the energy fluxes in all channels abruptly changes due to the changing energy distributions and interference patterns. Qualitatively this result follows from energy conservation in the interface layer and the following expression for the Poynting vector, constructed from the solutions in (7):

$$(S_1)_\alpha\sim \mathrm{Re}(k_{1,\alpha})=|k_{1,\alpha}|\left(\frac{\sqrt{\delta_a^2+(\mathrm{Im}\ \varepsilon^{(i_\alpha)})^2}+\delta_\alpha}{2\sqrt{\delta_\alpha^2+(\mathrm{Im}\ \varepsilon^{(i_\alpha)})^2}}\right)^{1/2}$$
$$=\begin{cases}|k_{1,\alpha}|\cos\dfrac{\psi_\alpha}{2} & \text{for } \delta_\alpha\geqslant 0\\ |k_{1,\alpha}|\sin\dfrac{\psi_\alpha}{2} & \text{for } \delta_\alpha<0,\end{cases} \tag{15}$$

where

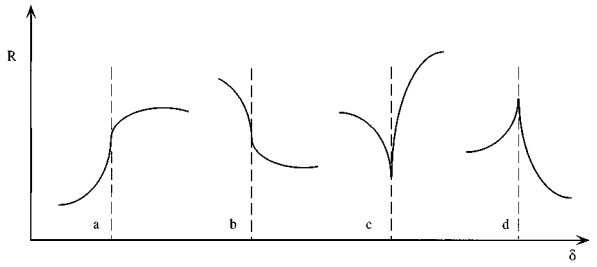

FIG. 2. General types of behavior (a), (b), (c), and (d), of solutions to Eq. (24) for the case of $\mathrm{Im}(\varepsilon^{(2)})=0$. The position of the threshold at $\delta_{\alpha_{\rm cr}}=0$ is denoted by the dashed line. In the case of $\mathrm{Im}(\varepsilon^{(2)})\neq 0$ the behavior near the singularities according to (24) would be rounded.

$$k_{1,\alpha}=|k_{1,\alpha}|\begin{cases}e^{i\psi_\alpha/2} & \text{for } \delta_\alpha>0\\ ie^{-i\psi_\alpha/2} & \text{for } \delta_\alpha<0\end{cases}$$

and

$$\cos\psi_\alpha=\frac{|\delta_\alpha|}{\sqrt{\delta_\alpha^2+(\mathrm{Im}\varepsilon^{(i_\alpha)})^2}},\quad 0\leqslant\psi_\alpha\leqslant\pi, \tag{16}$$

Note that $\psi_\alpha\cong\pi/2$ for $|\delta_\alpha|\ll\mathrm{Im}\varepsilon^{(i_\alpha)}$ and $\psi_\alpha\cong 0$ for $\delta_\alpha\gg\mathrm{Im}\varepsilon^{(i_\alpha)}$.

For the quantitative description of light scattering near the threshold $\delta_{\alpha_{\rm cr}}=0$ it is possible to use, with minor modifications, the threshold theory of multichannel wave scattering [9]. According to this theory,

$$r_{\alpha,\alpha_{\rm cr}}=M_\alpha\sqrt{k_{1,\alpha_{\rm cr}}} \quad \text{for } \alpha\neq\alpha_{\rm cr},$$
$$r_{\alpha,\alpha'}=r^0_{\alpha,\alpha'}+a_{\alpha,\alpha'}k_{1,\alpha_{\rm cr}} \quad \text{for } \alpha,\alpha'\neq\alpha_{\rm cr}, \tag{17}$$
$$r_{\alpha_{\rm cr},\alpha_{\rm cr}}=1,$$

where $k_{1,\alpha_{\rm cr}}$ is equal to

$$k_{1,\alpha_{\rm cr}}=\left[\varepsilon^{i_{\alpha_{\rm cr}}}\frac{\omega^2}{c^2}-\left(\overline{k_{0,\parallel}}+\frac{2\pi m_{\alpha_{\rm cr}}}{\Lambda}\overline{g}\right)^2\right]^{1/2}, \tag{17'}$$

$r^0_{\alpha,\alpha'}$ are the values of $r_{\alpha,\alpha'}$ at $k_{1,\alpha_{\rm cr}}=0$, and M_α and $a_{\alpha,\alpha'}$ are constants in the threshold approximation (that is up to higher terms in small quantity $|k_{1,\alpha_{\rm cr}}|$ near the threshold).

The condition of the energy balance on the interface boundaries $x_1=\pm l$ can be written, taking into account (15) and (16), as follows [10]:

$$\sum_{\tilde\alpha} r_{\alpha',\tilde\alpha}r^*_{\alpha,\tilde\alpha}f(\tilde\alpha)=[f(\tilde\alpha)-\kappa_\alpha]\delta_{\alpha,\alpha'}, \tag{18}$$

where κ_α is the supposedly small ($\kappa_\alpha\ll 1$) fraction of incident light energy absorbed in the thin layer $|x_1|<l$ and

$$f(\alpha)=\begin{cases}\cos\dfrac{\psi_\alpha}{2} & \text{for } \delta_\alpha\geqslant 0\\ \sin\dfrac{\psi_\alpha}{2} & \text{for } \delta_\alpha<0.\end{cases} \tag{19}$$

The angles ψ_α are small for all $\alpha \neq \alpha_{\rm cr}$ and correspondingly

$$f(\alpha) \cong \begin{cases} 1 & \text{for } \delta_\alpha \geqslant 0 \\ 0 & \text{for } \delta_\alpha < 0 \end{cases} \quad \text{for } \alpha \neq \alpha_{\rm cr}. \tag{20}$$

Note that $\psi_{\alpha_{\rm cr}}$ is not small and is equal approximately to $\pi/2$ in the threshold region where $\delta_{\alpha_{\rm cr}} \cong 0$ even if the conditions (6) are fulfilled. It follows from (17)–(20) that the relation (18) near the $\alpha_{\rm cr}$ threshold can be rewritten in the following form:

$$\sum_{\tilde{\alpha}} (r^0_{\alpha,\tilde{\alpha}} + a_{\alpha,\tilde{\alpha}} k_{1,\alpha_{\rm cr}})(r^{0*}_{\alpha',\tilde{\alpha}} + a^*_{\alpha',\tilde{\alpha}} k^*_{1,\alpha_{\rm cr}}) + M_\alpha M^*_{\alpha'} |k_{1,\alpha_{\rm cr}}| f(\alpha_{\rm cr}) = \delta_{\alpha,\alpha'}(1-\kappa_\alpha) \qquad \text{for } \alpha, \alpha' \neq \alpha_{\rm cr}, \tag{21}$$

where the sum is taken over all channels $\tilde{\alpha} \neq \tilde{\alpha}_{\rm cr}$ with $\delta_{\tilde{\alpha}} > 0$ and the dependence of κ_α on $k_{1,\alpha_{\rm cr}}$ is disregarded. The relation (21) at $\delta_{\alpha_{\rm cr}} < 0$, $\delta_{\alpha_{\rm cr}} > 0$ and at $k_{1,\alpha_{\rm cr}} = 0$ correspondingly takes the following forms:

$$\sum_{\tilde{\alpha}} (r^0_{\alpha,\tilde{\alpha}} \alpha^*_{\alpha',\tilde{\alpha}} e^{i\psi_{\alpha_{\rm cr}}/2} - r^{0*}_{\alpha',\tilde{\alpha}} a_{\alpha,\tilde{\alpha}} e^{-i\psi_{\alpha_{\rm cr}}/2}) + M_\alpha M^*_{\alpha'} \sin\frac{\psi_{\alpha_{\rm cr}}}{2} = 0 \quad \text{for } \delta_{\tilde{\alpha}=\alpha_{\rm cr}} < 0,$$

$$-i\sum_{\tilde{\alpha}} (r^0_{\alpha,\tilde{\alpha}} a^*_{\alpha',\tilde{\alpha}} e^{-i\psi_{\alpha_{\rm cr}}/2} - r^{0*}_{\alpha',\tilde{\alpha}} a_{\alpha,\tilde{\alpha}} e^{-i\psi_{\alpha_{\rm cr}}/2}) + M_\alpha M^*_{\alpha'} \cos\frac{\psi_{\alpha_{\rm cr}}}{2} = 0 \quad \text{for } \delta_{\tilde{\alpha}=\alpha_{\rm cr}} > 0, \tag{22}$$

$$\sum_{\tilde{\alpha}} (r^0_{\alpha,\tilde{\alpha}} a^*_{\alpha',\tilde{\alpha}} - r^{0*}_{\alpha',\tilde{\alpha}} a_{\alpha,\tilde{\alpha}}) = 0 \quad \text{for } k_{1,\alpha_{\rm cr}} = 0,$$

The solution of the equations (22) is

$$\begin{aligned} a_{\alpha,\alpha'} &= -\tfrac{1}{2} M_\alpha M_{\alpha'}, \\ M_\alpha &\sum_\alpha r^0_{\alpha,\tilde{\alpha}} M^*_{\tilde{\alpha}}, \end{aligned} \tag{23}$$

The results in (23) are analogous to the those found in the threshold theory of multichannel wave scattering on a localized scatterer [8,9]. The solution (23) together with (16) and (17) allows us to express near the thresholds the reflection coefficients $R_{\alpha,\alpha'} = |r_{\alpha,\alpha'}|^2$ and phases $\arg(r_{\alpha,\alpha'})$ through the coefficients M_α and $r^0_{\alpha,\alpha'}$ as follows:

$$\begin{aligned} R_{\alpha,\alpha'} = |r_{\alpha,\alpha'}|^2 = |r^0_{\alpha,\alpha'}|^2 - \tfrac{1}{2}[&\mathrm{Re}(r^0_{\alpha,\alpha'} M^*_\alpha M^*_{\alpha'}) \sqrt{\tfrac{1}{2}[\sqrt{\delta^2_{\alpha_{\rm cr}} + (\mathrm{Im}\varepsilon^{(i_{\alpha_{\rm cr}})})^2} + \delta_{\alpha_{\rm cr}}]} \\ &- \mathrm{Im}(r^0_{\alpha,\alpha'} M^*_\alpha M^*_{\alpha'}) \sqrt{\tfrac{1}{2}[\sqrt{\delta^2_{\alpha_{\rm cr}} + (\mathrm{Im}\varepsilon^{(i_{\alpha_{\rm cr}})})^2} - \delta_{\alpha_{\rm cr}}]}\,], \\ \arg(r_{\alpha,\alpha'}) = \arg(r^0_{\alpha,\alpha'}) &- \mathrm{Re}\left(\frac{M_\alpha M_{\alpha'}}{r^0_{\alpha,\alpha'}}\right) \sqrt{\tfrac{1}{2}[\sqrt{\delta^2_{\alpha_{\rm cr}} + (\mathrm{Im}\varepsilon^{(i_{\alpha_{\rm cr}})})^2} + \delta_{\alpha_{\rm cr}}]} \\ &+ \mathrm{Im}\left(\frac{M_\alpha M_{\alpha'}}{r^0_{\alpha,\alpha'}}\right) \sqrt{\tfrac{1}{2}(\sqrt{\delta^2_{\alpha_{\rm cr}} + (\mathrm{Im}\varepsilon^{(i_{\alpha_{\rm cr}})})^2} - \delta_{\alpha_{\rm cr}})} \quad \text{for } \alpha, \alpha' \neq \alpha_{\rm cr}, \end{aligned} \tag{24}$$

The result (24) can be summarized as follows. Near the threshold $\delta_{\alpha_{\rm cr}} = 0$ the reflection coefficients and phases of all scattered and transmitted waves have singular behavior of the type depicted in Fig. 2 with coefficients constructed from the real and imaginary parts of $r^0_{\alpha,\alpha'}$, $M^*_\alpha M^*_{\alpha'}$, and $M_\alpha M_{\alpha'}/r^0_{\alpha,\alpha'}$. The position of the singularity depends only upon the bulk dielectric properties [10].

Until now, all calculations have been made in the framework of the general threshold approximation. In order to estimate the values of the combinations of the constants $r^0_{\alpha,\alpha'}$, M_α, and $M_{\alpha'}$ in (24) we will use the perturbation theory in the parameter l/λ. According to the ''golden rule'' of perturbation theory in the continuous spectrum [11] the scattering amplitudes $r_{\alpha,\alpha'}$ from unit surface area are equal to [12]

$$r_{\alpha,\alpha'} \underset{S\to\infty}{=} \frac{\omega}{(2\pi)^{1/2}} \frac{1}{S} \sum_{i,j=1}^{3} \int_S [E^{F,(-)}_{\alpha,i}(\overline{x})]^* \delta\varepsilon_{ij}(\overline{x},\omega) E^{F,(+)}_{\alpha',j}(\overline{x}) d\overline{x}^3 \quad \text{for } m_\alpha \neq m_{\alpha'}, \tag{25}$$

where S is the surface area and the functions $E^F_{\alpha,\alpha'}(\overline{x})$ are Fresnel's solutions of the unperturbed problem with a stepwise uniform interface which have the form (12) and (14) with coefficients $r^0_{\alpha,\alpha'}$ equal to

$$r^0_{\alpha,\alpha'}=r^F_\alpha \quad \text{for } \alpha=\alpha',$$

$$r^0_{\alpha,\alpha'}=\sqrt{k^{(1)}_\alpha/k^{(1)}_{\alpha'}}(1-r^F_\alpha)\begin{cases}1 & \text{for } i_\alpha\neq i_{\alpha'};\ \zeta_\alpha=\zeta_{\alpha'}=s;\ m_\alpha=m_{\alpha'}\\ \sqrt{\varepsilon_\alpha/\varepsilon_{\alpha'}} & \text{for } i_\alpha\neq i_{\alpha'};\ \zeta_\alpha=\zeta_{\alpha'}=p;\ m_\alpha=m_{\alpha'},\end{cases} \tag{26}$$

$$r^0_{\alpha,\alpha'}=0 \quad \text{for } \zeta_\alpha\neq\zeta_{\alpha'} \text{ and/or } m_\alpha\neq m_{\alpha'},$$

where r^F_α are Fresnel's reflection amplitudes [13]:

$$r^F_\alpha=\frac{\varepsilon^{(\tilde{i}_\alpha)}[(\omega^2/c^2)\varepsilon^{(i_\alpha)}-(\overline{k^0_\parallel}+m_\alpha\overline{q})^2]^{1/2}-\varepsilon^{(i_\alpha)}[(\omega^2/c^2)\varepsilon^{(\tilde{i}_\alpha)}-(\overline{k^0_\parallel}+m_\alpha\overline{q})^2]^{1/2}}{\varepsilon^{(\tilde{i}_\alpha)}[(\omega^2/c^2)\varepsilon^{(i_\alpha)}-(\overline{k^0_\parallel}+m_\alpha\overline{q})^2]^{1/2}+\varepsilon^{(i_\alpha)}[(\omega^2/c^2)\varepsilon^{(\tilde{i}_\alpha)}-(\overline{k^0_\parallel}+m_\alpha\overline{q})^2]^{1/2}} \quad \text{for } \zeta_\alpha=p,$$

$$r^F_\alpha=\frac{[(\omega^2/c^2)\varepsilon^{(i_\alpha)}-(\overline{k^0_\parallel}+m_\alpha\overline{q})^2]^{1/2}-[(\omega^2/c^2)\varepsilon^{(\tilde{i}_\alpha)}-(\overline{k^0_\parallel}+m_\alpha\overline{q})^2]^{1/2}}{[(\omega^2/c^2)\varepsilon^{(i_\alpha)}-(\overline{k^0_\parallel}+m_\alpha\overline{q})^2]^{1/2}+[(\omega^2/c^2)\varepsilon^{(\tilde{i}_\alpha)}-(\overline{k^0_\parallel}+m_\alpha\overline{q})^2]^{1/2}} \quad \text{for } \zeta_\alpha=s, \tag{26'}$$

$$(\tilde{i}_\alpha)=\begin{cases}1 & \text{for } (i_\alpha)=2\\ 2 & \text{for } (i_\alpha)=1.\end{cases}$$

The coefficient $\omega/(2\pi)^{1/2}$ in (25) corresponds to the kinematics of scattering by an infinite flat interface and is different from the analogous coefficient in the perturbation theory of wave scattering by a scatterer localized in all dimensions [11].

The Fresnel's solutions of light scattering problems have continuous across the interface components of the field $E^F_\alpha(\overline{x})$ parallel to the interface and a normal to the interface component of the displacement $D^F_{\alpha,1}(\overline{x})=\varepsilon_0(x_1)E^F_{\alpha,1}(\overline{x})$. Near the interface these continuous field components change on relatively large (in the discussed perturbation theory) distances $\lambda\gg l$, which allows us to take them out of the integral over dx_1 in (25) at the point $x_1=0$ on the interval $|x_1|<l$ where $\delta\varepsilon_{ij}(\overline{x})$ is concentrated:

$$r_{\alpha,\alpha'}\underset{S\to\infty}{\cong}\frac{\omega}{Sc}\int_s d^2x_\parallel\Bigg\{\{[\overline{E^{F,-}_{\alpha,\parallel}}(\overline{x})]^*\overline{E^{F,+}_{\alpha',\parallel}}(\overline{x})\}|_{x_1=0}\int_{-\infty}^{\infty}dx_1\ \delta\varepsilon(\overline{x},\omega)$$
$$-\{[\overline{E^{F,-}_{\alpha,1}}(\overline{x})\varepsilon^{(i_\alpha)}]^*\overline{E^{F,+}_{\alpha',1}}(\overline{x})\varepsilon^{(i_{\alpha'})}\}\Big|_{x_1=0}\int_{-\infty}^{\infty}dx_1\,\delta\frac{1}{\varepsilon(\overline{x},\omega)}\Bigg\}+O\left(\left(\frac{l}{\lambda}\right)^2\right). \tag{27}$$

We have supposed in (27), for simplicity, that $\delta\varepsilon_{ij}(\overline{x})$ is symmetrical:

$$\delta\varepsilon_{ij}(\overline{x})=\delta_{ij}\delta\varepsilon(\overline{x}). \tag{28}$$

The function $\delta 1/\varepsilon(\overline{x},\omega)$, introduced in (27), which determines the scattering amplitudes of p-polarized light, has the following form:

$$\delta\frac{1}{\varepsilon(\overline{x},\omega)}\equiv\frac{-1}{\varepsilon^2(\overline{x},\omega)}\,\delta\varepsilon(\overline{x},\omega)=\sum_{n=-\infty}^{\infty}\tilde{\delta}\frac{1}{\varepsilon}(x_1,n,\omega)e^{in(\overline{q\cdot x_\parallel})}\cong\frac{1}{\varepsilon(\overline{x},\omega)}-\frac{1}{\varepsilon_0(x_1,\omega)}. \tag{29}$$

The expressions (27) can be transformed further taking into account that

$$|E^{F,+}_{\alpha,i}(\overline{x})|_{x_1=0}=(1+r^F_\alpha)\frac{1}{\sqrt{k_{1,\alpha}}}\frac{\sqrt{4\pi\omega}}{c}. \tag{30}$$

Introducing (30) into (27) we find with the help of (2), (7), (12), (13a), (14), and (29) that

$$r_{\alpha,\alpha'}=\frac{16\pi\omega^2}{c^2}\frac{\overline{k_{\parallel,\alpha}}\cdot\overline{k_{\parallel,\alpha'}}}{\sqrt{\overline{k^2_{\parallel,\alpha}}\cdot\overline{k^2_{\parallel,\alpha'}}}}\frac{\sqrt{k^*_{1,\alpha}k_{1,\alpha'}}}{(k_{1,\alpha'}+k_{1,\tilde{\alpha}'})(k^*_{1,\alpha}+k^*_{1,\tilde{\alpha}})}\frac{1}{2\pi}\int_{-\infty}^{\infty}dx_1\ \delta\tilde{\varepsilon}(x_1,m_\alpha-m_{\alpha'},\omega) \quad \text{for } \zeta_\alpha=\zeta_{\alpha'}=s,$$

$$r_{\alpha,\alpha'}=\frac{16\pi(m_{\alpha'}-m_\alpha)|\overline{k^0_\parallel}\times\overline{q}|k_{1,\alpha}\omega/c}{\sqrt{\varepsilon^{(i_\alpha)}(\overline{k_{\parallel,\alpha}})^2(\overline{k_{\parallel,\alpha'}})^2}}\frac{(\varepsilon^{(i_\alpha)}\sqrt{k_{1,\alpha}})^*\sqrt{k_{1,\alpha'}}}{(\varepsilon^{(\tilde{i}_\alpha)}k_{1,\alpha}+\varepsilon^{(i_\alpha)}k_{1,\tilde{\alpha}})^*(k_{1,\alpha'}+k_{1,\tilde{\alpha}'})}\frac{1}{2\pi}\int_{-\infty}^{\infty}dx_1\ \delta\tilde{\varepsilon}(x_1,m_\alpha-m_{\alpha'},\omega)$$

$$\text{for } \zeta_\alpha=p,\ \zeta_{\alpha'}=s, \tag{31}$$

$$r_{\alpha,\alpha'}=\frac{16\pi\varepsilon^{(\tilde{i}_{\alpha'})}\sqrt{(\varepsilon^{(i_\alpha)}k_\alpha)^*(\varepsilon^{(i_{\alpha'})}k_{\alpha'})}}{\sqrt{\overline{k^2_{\parallel,\alpha'}}\cdot\overline{K^2_{\parallel,\alpha}}}}\frac{1}{(\varepsilon^{(\tilde{i}_\alpha)}k_{1,\alpha}+\varepsilon^{(i_\alpha)}k_{1,\tilde{\alpha}})^*}\frac{1}{(\varepsilon^{(\tilde{i}_{\alpha'})}k_{1,\alpha'}+\varepsilon^{(i_{\alpha'})}k_{1,\tilde{\alpha}'})}\left\{(\overline{k_{\parallel,\alpha}}\cdot\overline{k_{\parallel,\alpha'}})k_{1,\alpha}k_{1,\alpha'}\right.$$

$$\left.\times\int_{-\infty}^{\infty}dx_1\ \delta\tilde{\varepsilon}(x_1,m_\alpha-m_{\alpha'},\omega)+\overline{k^2_{\parallel,\alpha}}\cdot\overline{k^2_{\parallel,\alpha'}}\int_{-\infty}^{\infty}dx_1\ \delta\frac{\tilde{1}}{\varepsilon}(x_1,m_\alpha-m_{\alpha'},\omega)\right\}\quad\text{for }\zeta_\alpha=\zeta_{\alpha'}=p.$$

The expression for the transition amplitudes for $\zeta_\alpha=s$, $\zeta_{\alpha'}=p$ can be found from (31) with the help of (13). It follows from (17) and (31) that in the approximation (4):

$$M_\alpha=\frac{1}{\sqrt{\varepsilon^{\tilde{i}_{\alpha_{\rm cr}}}-\varepsilon^{i_{\alpha_{\rm cr}}}}}\frac{1}{\sqrt{2\pi}}\int_{-\infty}^{\infty}dx_1\ \delta\varepsilon(x_1,m_\alpha-m_{\alpha_{\rm cr}},\omega)\quad\text{for }\zeta_\alpha=s,$$

$$M_\alpha=16\pi\left(\frac{\varepsilon^{(i_{\alpha_{\rm cr}})}}{\varepsilon^{(\tilde{i}_{\alpha_{\rm cr}})}}\right)^{1/2}\frac{\sqrt{(k^2_{\parallel,\alpha})^*(\varepsilon^{i_\alpha}k_\alpha)^*}}{(\varepsilon^{(\tilde{i}_\alpha)}k_{1,\alpha}+\varepsilon^{(i_\alpha)}k_{1,\tilde{\alpha}})}\Bigg|_{\delta_{\alpha_{\rm cr}}=0}\frac{1}{\sqrt{\varepsilon^{\tilde{i}_{\alpha_{\rm cr}}}-\varepsilon^{i_{\alpha_{\rm cr}}}}}\int_{-\infty}^{\infty}dx_1\ \delta\frac{\tilde{1}}{\varepsilon}(x_1,m_\alpha-m_{\alpha_{\rm cr}},\omega)\quad\text{for }\zeta_\alpha=p,\tag{32}$$

The expressions (32) indicate that the qualitatively different threshold behavior of the s- and p-polarized light scattering can be expected in the case of metallic gratings on dielectric substrates or vice versa. When the grating and substrate dielectric functions have real parts of different signs for different values of $\overline{x}$ the continuation of the function $\delta 1/\varepsilon(\overline{x},\omega)$ into the complex plane of x_1 becomes infinite at some point $x_1-x_1^0$ with the distance from the real axis $\mathrm{Im}x_1^0$ proportional to the value of the imaginary component of $\delta\varepsilon(\overline{x},\omega)$. This effect can be interpreted as a result of the formation of local surface plasmon resonances. The corresponding enhancement of the imaginary component of the integral

$$\int_{-\infty}^{\infty}dx\ \delta\frac{\tilde{1}}{\varepsilon}(x_1,m_\alpha-m_{\alpha'},\omega)\tag{33}$$

leads to the complex values of M_α with comparable real and imaginary part even if the imaginary part of $\delta\tilde{\varepsilon}$ is substantially smaller than the real part. It follows from (24), (27), and the structure of (33) that in particular in the expressions for the specular p-wave scattering, the coefficients in terms in (24) proportional to $\{\frac{1}{2}[\sqrt{\delta^2_{\alpha_{\rm cr}}+(\mathrm{Im}\varepsilon^{(i_{\alpha_{\rm cr}})})^2}+\delta_{\alpha_{\rm cr}}]\}^{1/2}$ and $\{\frac{1}{2}[\sqrt{\delta^2_{\alpha_{\rm cr}}+(\mathrm{Im}\varepsilon^{(i_{\alpha_{\rm cr}})})^2}-\delta_{\alpha_{\rm cr}}]\}^{1/2}$, respectively, have to be of the same order of magnitude and negative [Fig. 2(d)]. In the case of the s-wave scattering the corresponding coefficients in the term proportional to $\{1/2[\sqrt{\delta^2_{\alpha_{\rm cr}}+(\mathrm{Im}\varepsilon^{(i_{\alpha_{\rm cr}})})^2}+\delta_{\alpha_{\rm cr}}]\}^{1/2}$ must be substantially larger than the coefficients in the second term proportional to $\{\frac{1}{2}[\sqrt{\delta^2_{\alpha_{\rm cr}}+(\mathrm{Im}\varepsilon^{(i_{\alpha_{\rm cr}})})^2}-\delta_{\alpha_{\rm cr}}]\}^{1/2}$ [Fig. 2(a)].

III. DESCRIPTION OF EXPERIMENTS

The principal experimental scheme is given in Figs. 1 and 3, with Fig. 3 detailing the experimental configuration and apparatus. As shown in Fig. 3, the diffraction grating substrate was mounted into a sample cell placing the grating in contact with the analyte medium. Grating substrates consisted of 1-in.-diam $\frac{3}{16}$-in-thick fused silica disks (Esco) with standard photolithographic chrome mask layers of 1000-Å thickness deposited on the disks (Nanofilm, Inc.). A Lloyd's mirror configuration [1] was used to record interference fringes in a spin-coated positive photoresist from the spatially filtered, expanded, and collimated output of an argon ion laser. Each substrate was then developed and etched to the silica, forming a transmission grating on each. The grating period of the substrates used in these studies was measured to be 829.4 ± 0.7 nm.

In order to characterize the response of GLRS to bulk dielectric modulations and correlate the response with theory, separate experiments were carried out: initial first-order diffraction analysis and zeroth-order analysis via a dispersive monochromator. The white light source for these experiments was a tungsten bulb with a dc voltage source that was coupled into a 220-μm-diam silica fiber optic. The fiber output was collimated via a fiber coupled achromatic lens and polarized with a Glan Taylor polarizing prism to either transverse electric (s) or transverse magnetic (p). The collimated light was incident on the backside of the substrate, and thus passed through the fused silica to the grating.

For the first-order reflection, the grating acted as the dispersing element, and the $m=-1$ reflected diffraction order was imaged on a 512-element fiber-optic window photodiode array (EG&G Reticon). The image was spectrally calibrated via bandpass filters and exhibited a linear dependence of wavelength on diode number, with approximately 120 nm imaged on the array. The beam diameter was approximately 5 mm, and the diffracted light was focused on the detector with a 63-mm focal length achromatic lens.

The zeroth-order optical system consisted of an optimized version of the system used in the first-order experiments. The output of the fiber was collimated via a bulk optic achromat collimator and the beam size minimized using an iris aperture to reduce off-axis light incident on the grating. The incident polarization state was set via a Glan Taylor cube polarizer. The reference beam was captured via a ball-lens coupled collection fiber optic as a specular reflection off the first surface of the substrate or at the output of the collimator, removing a portion of the poorly collimated light at the limit

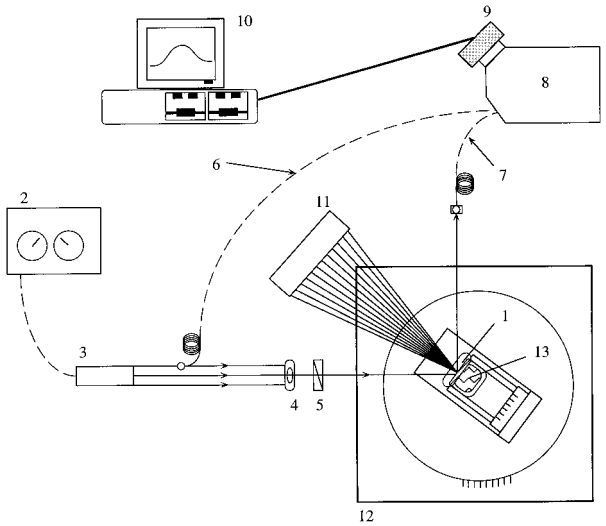

FIG. 3. Experimental apparatus for GLRS experiments. (1) grating substrate with period of 829.4. nm, (2) dc tungsten-halogen source, fiber bundle coupled to (3) achromat collimation lens, (4) iris, (5) Glan Taylor polarizer, (6) microsphere coupled reference fiber optic, (7) microsphere coupled sample fiber optic collecting the specular reflection off of the grating-sample interface, (8) McPherson monochromator with stacked fiber input, (9) SBIG CCD array camera, (10) 486 PC for data acquisition and transfer, (11) EG&G 512-element linear diode array with fiber optic window collecting the first-order diffraction, focusing optics not shown, (12) dual axis rotation stage, (13) Teflon sample cell (PEEK flow cell in first-order experiments).

of the clear aperture of the lens but not affecting the light incident on the grating. The grating-substrate interface specular reflection was collected as the sample beam via a similar collection fiber.

These two collection fibers were coupled into a McPherson 218 monochromator via aperture matching optics and adjustable slit as a stacked pair, and these dispersed images were vertically resolved onto a Santa Barbara Instruments Group ST-6 charge-coupled device (CCD) camera placed in the image plane of the monochromator. The wavelength range of the spectrometer was selectable via a selection dial and the bandwidth of the instrument was 77 nm at any one setting on the monochromator. The resolution of the spectrometer system was 1.9 nm for an entrance slit width of 500 μm.

The grating substrate was mounted on a dual axis rotation stage with the incident angular resolution of 0.083° and an azimuthal angular resolution of 0.5° (see Fig. 3). The sample was pumped using a peristaltic into a sandwich-type flow cell and stopped during data acquisition for the first-order experiments. In the zeroth-order experiments, the sample was placed in a 2-mL Teflon sample holder, pressure fitted, and sealed with a Parafilm gasket against the grating side of the substrate; the sample was introduced via a pipette.

The set of experiments corresponding to the case of low absorption [$\mathrm{Im}(\epsilon^{(2)})\sim 0$] were performed with ethanol:water solutions. The refractive index of each ethanol:water solution was measured using an Abbé refractometer at various temperatures and the refractive index temperature dependence and dispersion calculated for each solution. The cleaned substrate (grating period 829.4±.76 nm) was mounted in the substrate holder-flow cell, the incident angle set to 36°, and the stage locked. The azimuthal angle was set to 0° and the azimuth stage locked. The polarization was initially set to *p* polarization. Measurements were taken in a static format in order to remove flow effects within the cell. The sample was introduced into the cell with a peristaltic pump, and the flushing sequence was a combination of well-defined flow and stop flow steps designed to ensure complete flushing, minimizing contamination from previous runs. The ethanol solutions were run in random order with a water reference taken at the outset. First-order diffraction was were collected as full array images at 5-s intervals, with 10 scans of the array taken for each solution. The polarizer was rotated to *s* polarization and the ethanol samples run again in random order.

In addition, the cleaned substrate was mounted in the substrate-Teflon sample holder assembly, the incident angle set to 36.17°, azimuthal angle was set to 0°, and polarization set to *p* polarization. Between samples, the cell was rinsed and aspirated with copious amounts of deionized water and then rinsed twice with sample. Twenty scans of the array were taken for each sample at an integration time of 2 s, and a twenty scan dark current measurement was subtracted manually at the data analysis stage. The nine ethanol:water solutions were run in random order. The polarizer was then rotated to achieve *s* polarization and the ethanol samples run again in random order.

Six solutions of methylene blue in water were prepared in order to test the GLRS response to absorbing species. The absorbances of methylene blue samples were measured on a Hewlett Packard 8540A UV/Vis diode array spectrometer in a cell fashioned from two fused silica plates and a thin Teflon spacer, and then converted to the corresponding equivalent 1-cm path-length absorbances. The thin cell thickness was inferred from a comparison of the 1-cm cuvette measurements and thin cell measurements using the two least concentrated solutions. The system was initially set to an incident angle of 37.11°, azimuthal angle of 0°, and *p* polarization. The cell was cleaned with deionized water, rinsed with 0.1*M* nitric acid, rinsed again with water, and then the first sample was run. Subsequent samples were run, again preceded by a nitric acid rinse, water rinse, and two volumes of sample rinse. The methylene blue samples were run in random order at three different angles of incidence: 37.11°, 34.98°, and 30.62°, respectively.

Each sample generated a single 10×512 matrix for the first-order diffraction runs. Each sample matrix was averaged and then subtracted from the water sample data to generate a difference spectrum with respect to water. Each zeroth-order sample run generated two 20×750 matrices of sample and reference data that were averaged to obtain 1×750 vectors of sample and corresponding reference spectra, which were then dark corrected. An 11-point smoothing filter was applied to each reference spectrum while the sample spectra were unaltered except for dark correction. Relative reflection spectra were calculated for each run by calculating the ratio of each sample spectrum to its corresponding reference spectrum. The derivatives of the specular relative reflection coefficients were calculated using a 71-point Savitsky-Golay first derivative filter, with the peak maxima located for comparison with theoretical predictions.

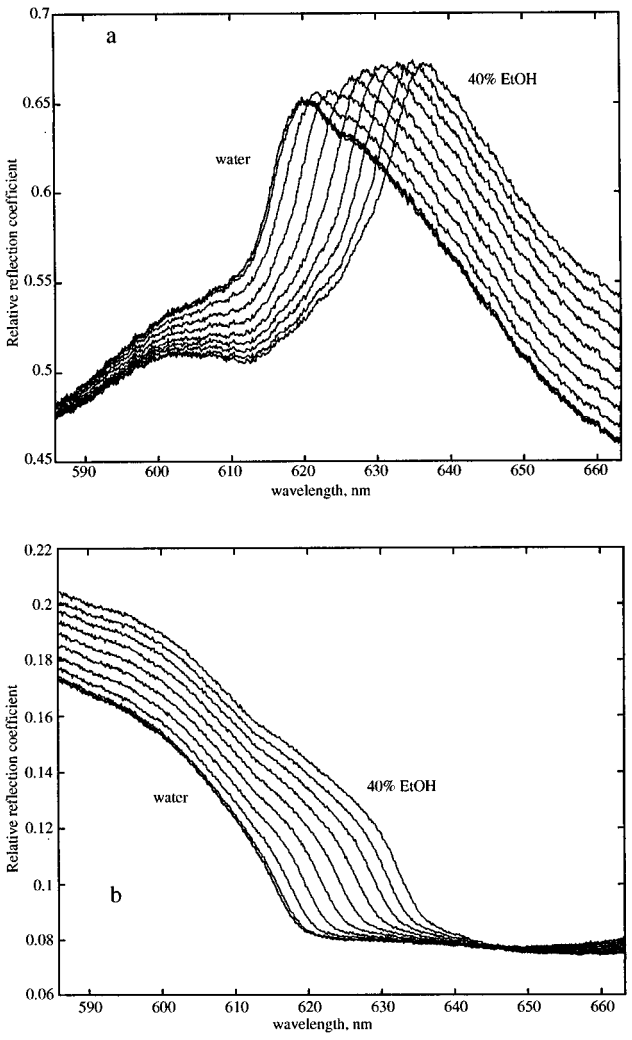

FIG. 4. GLRS relative reflection coefficients calculated from experimental reflected intensities for ethanol:water solutions, *p* polarization (a) and *s* polarization (b). Ethanol was prepared from absolute ethanol (McCormick, Lot No. CO3512) and deionized water in the following concentrations: 1%, 5%, 10%, 15%, 20%, 25%, 30%, 35%, and 40% vol/vol. The sodium *d*-line refractive index range for these samples is 1.3321 for water to 1.3530 for 40% ethanol. The singularity shifts to higher wavelengths for increases in refractive index due to increases in ethanol concentration where the threshold is taken as the point of highest slope.

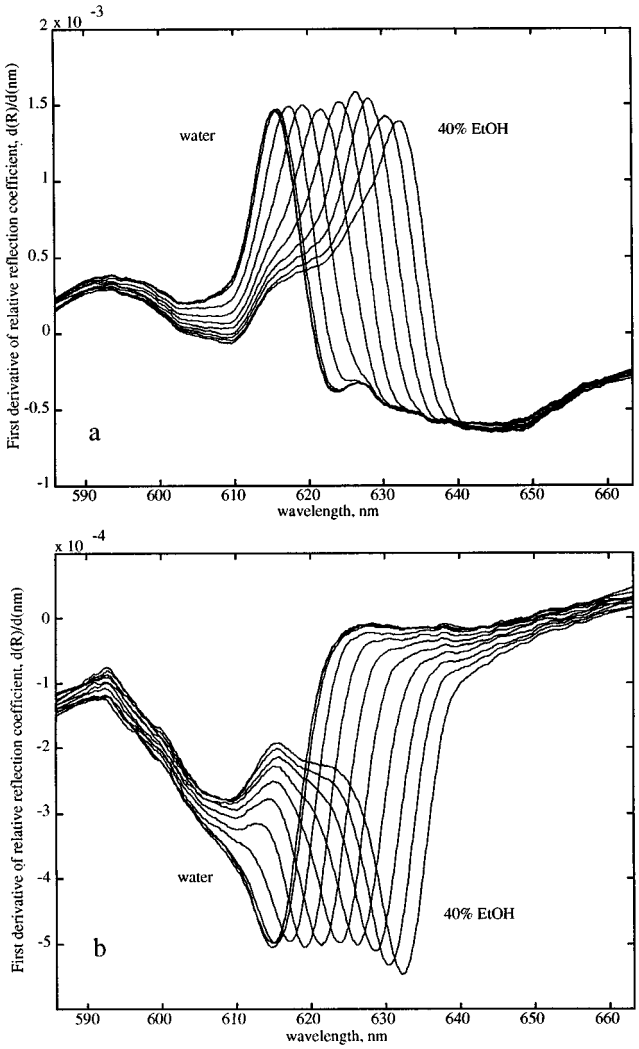

FIG. 5. GLRS derivative of relative reflection coefficients calculated for ethanol:water solutions, *p* polarization (a), and *s* polarization (b), 71-point Savitsky-Golay derivative filter applied to 750 data points. The peak of the derivative is taken as the singularity.

IV. RESULTS AND DISCUSSION

The purpose of the experiments was to analyze the form of the reflection coefficients and find the positions of the thresholds associated with the theory presented. For all experiments, the critical diffraction order undergoing the transformation was the $m_{\rm cr}=1$ transmitted order for $i_{\alpha_{\rm cr}}=2$. Experiments were carried out for high and low sample medium absorption and two transmitted diffraction orders were monitored: the zeroth order (specular reflection), and the $m=-1$ reflected order reflected into medium(0) (air). The form of the reflection coefficient in Eq. (24) (and Fig. 2) indicate the existence of a singular reflected intensity dependence in wavelength space on a number of parameters: wavelength (λ), grating period (Λ), angle of incident (θ), angle between the plane of incidence and direction of grating periodicity (γ), and dielectric function of the sample medium $[\epsilon^{(2)}(\omega)]$. The threshold singularity is defined by Eq. (14), which may be rewritten to include the experimentally relevant quantities listed above as follows:

$$\delta_{\alpha_{\rm cr}}=\mathrm{Re}(\varepsilon^{(2)})-\left[\sin^2\theta+m^2\left(\frac{\lambda}{\Lambda}\right)^2+2m\,\frac{\lambda}{\Lambda}\sin\theta\,\cos\gamma\right]=0, \tag{34}$$

where $\cos\gamma=\overline{k_{\|}}\cdot\overline{g}/|\overline{k_{\|}}|$.

For all experiments the angle between the plane of incidence and the direction of the grating periodicity was set equal to zero. As the experiments were performed with a white light source and a spectrometer, the selection of the incidence angle, the grating period, and the refractive index yield a threshold at a specific wavelength. The experimental verification of this is shown in Figs. 4(a) and 4(b) for orthogonal polarizations *s* and *p*. The threshold wavelength is

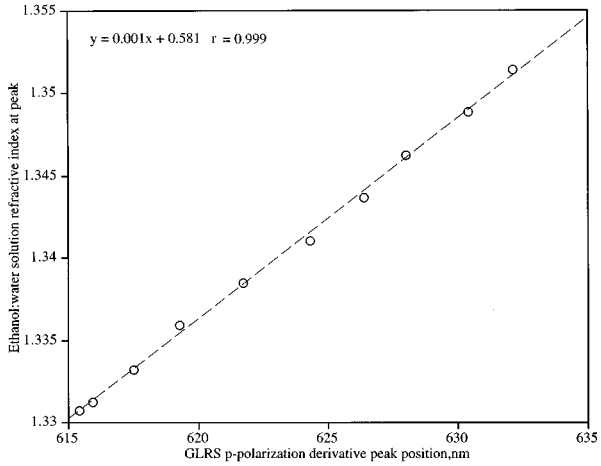

FIG. 6. Ethanol:water solution refractive indices (corrected for dispersion and temperature) plotted against the threshold wavelengths obtained from the peak positions from the p polarization derivative plots. The linearity is expected and the values of the slope and intercept agree with the experimental parameters: at $\delta_{\alpha_{cr}}=0$, $\sqrt{\mathrm{Re}\,\varepsilon^{(2)}}=\sin\theta+(m_{cr}/\Lambda)\lambda$, from the description of the experiments, $m_{cr}/\Lambda=0.0012$, and $\sin(36.167°)=0.590$, in agreement with the linear regression of the data shown here.

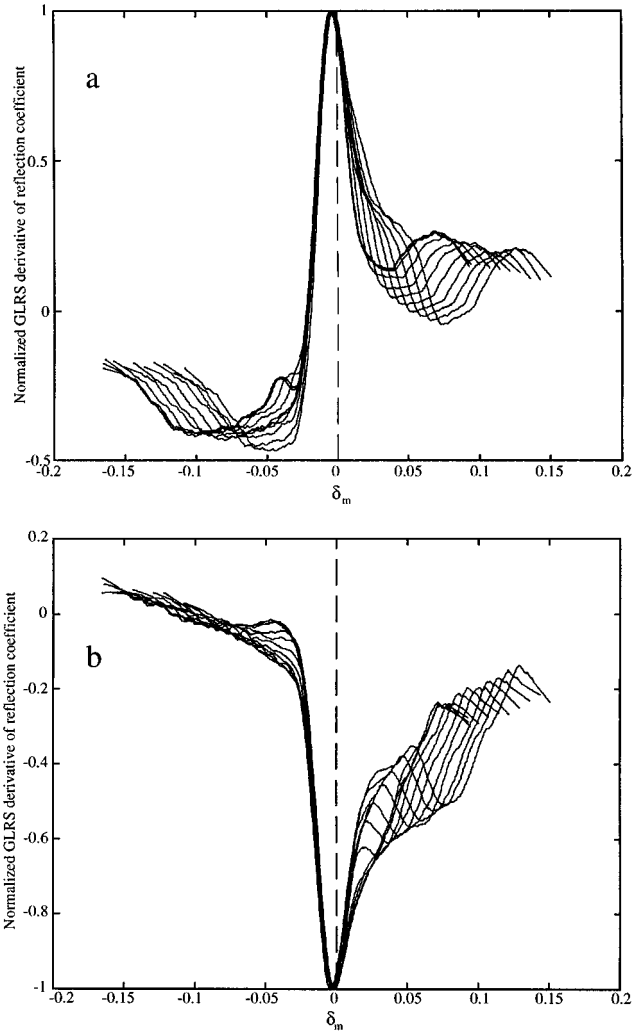

FIG. 7. Relative reflection coefficients for the ethanol:water sample plotted against calculated from experimental values of refractive index (corrected for dispersion), angle of incidence, grating period, and wavelength for incident p polarization (a) and s polarization (b). The peaks occur, in theory, at $\delta_{\alpha_{cr}}=0$, and the offset here in both polarizations is due to the error in determining the incident angle.

taken as the point of highest slope in the relative reflection coefficient data, and the forms of the data agree with the predicted forms depicted in Fig. 2. In order to compare the positions of the experimental thresholds with those predicted with theory, the derivatives of the reflection coefficients over δ or λ can be analyzed taking the peak position as the threshold. The corresponding reflection coefficient derivatives are plotted in Figs. 5(a) and 5(b), again for orthogonal polarizations s and p. The peak positions in wavelength were determined and plotted versus the corresponding refractive index of the ethanol:water solution corrected for dispersion and temperature. The linear dependence of threshold wavelength demonstrated in Fig. 6 is expected as the function in (34) exhibits a linear relationship between wavelength and $\mathrm{Re}(\varepsilon^{(2)})$ when other experimental parameters are held constant.

In order to further correlate the response of GLRS with theory, the function $\delta_{\alpha_{cr}}$ was calculated from experimental values of refractive index, dispersion, angle of incidence, grating period, and wavelength. The zero crossing for this function shifts to higher wavelengths with increases in refractive index. The derivatives of the reflection coefficients were plotted against each corresponding model threshold function. It is expected that each peak would occur at $\delta_{\alpha_{cr}}=0$, and this is demonstrated in Figs. 7(a) and 7(b). Normalization of each peak to unit height removed the underlying grating function, and thus simplified visual comparison of peak positions. The offset from $\delta_{\alpha_{cr}}=0$ and the spread around a mean value of $\delta_{\alpha_{cr}}$ result from errors in determining the angle of incidence and the subsequent use of dispersion tables to calculate the dispersion for each ethanol:water solution.

The general shape of the derivatives away from the singularity is due to the wavelength dependence of the coefficients in (24), $\mathrm{Re}(r^0_{\alpha,\alpha'}M^*_\alpha M^*_{\alpha'})$ and $\mathrm{Im}(r^0_{\alpha,\alpha'}M^*_\alpha M^*_{\alpha'})$. It is important to note the interesting symmetry about these thresholds where the p-polarization relative reflection coefficient curves are mirror images of the s polarization. This arises from the orthogonal nature of polarization response as well as from the polarization-dependent grating function away from the thresholds as detailed by the functions describing the coefficients in (24). We did not explicitly calculate the values of $\mathrm{Re}(r^0_{\alpha,\alpha'}M^*_\alpha M^*_{\alpha'})$ and $\mathrm{Im}(r^0_{\alpha,\alpha'}M^*_\alpha M^*_{\alpha'})$ in this paper, but the qualitative differences in polarization response agree with the expected differences arising from the perturbation theory in the parameter l/λ.

The general nature of the reflection coefficient derivation and the connection between scattered reflected and transmitted light predicts that the threshold has to be observed in any monitored diffraction order. To check this prediction, the first-order diffraction reflection was monitored in response to

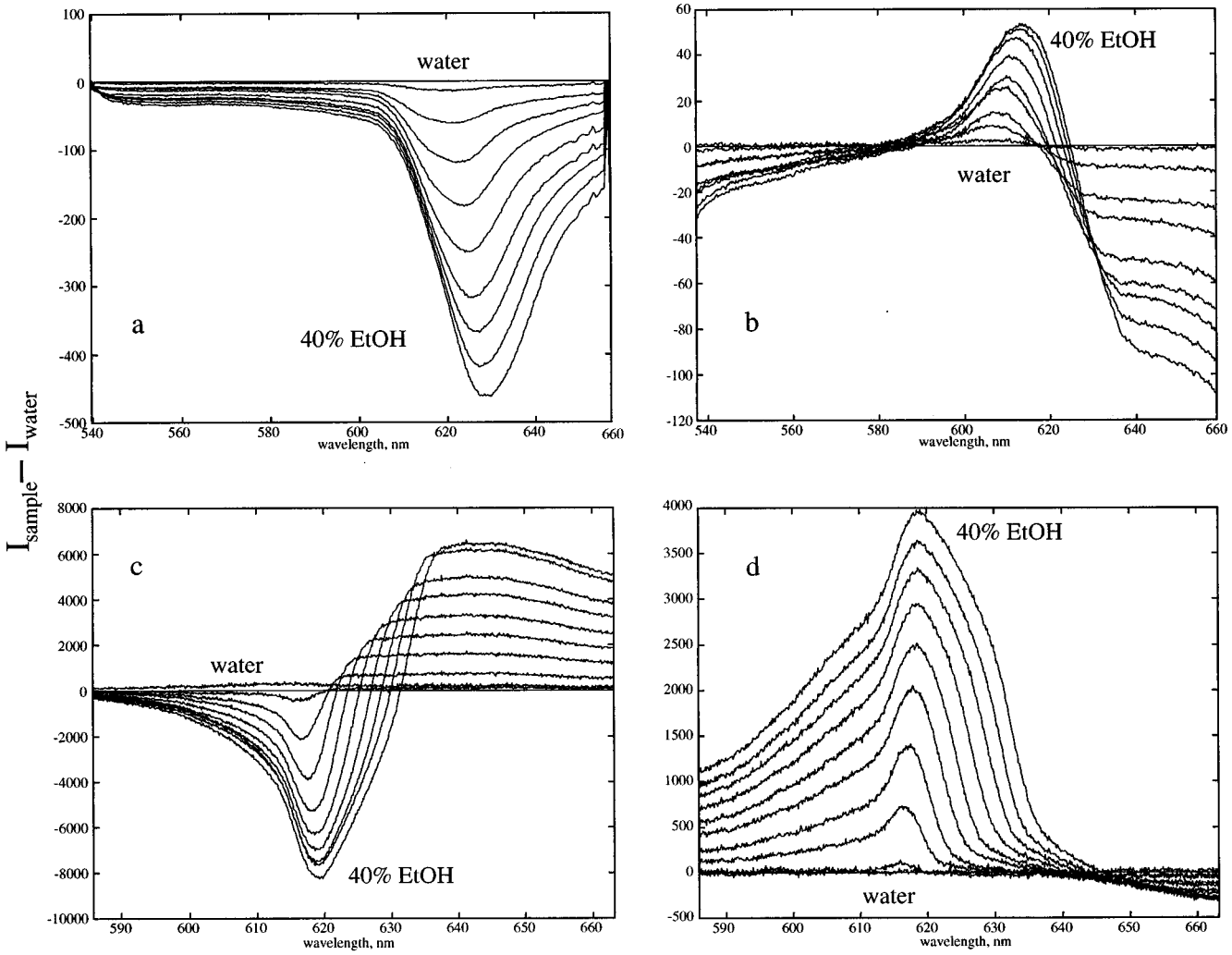

FIG. 8. Reflected intensity response to ethanol:water solutions, referenced to the water response for monitored (a) first-order *p* polarization, (b) first-order *s* polarization, (c) zeroth-order *p* polarization, and (d) zeroth-order *s* polarization incident. The similarity in response indicates the threshold is present in all diffracted reflected orders, but here the peaks do not correspond to the thresholds. In addition, the thresholds occur at different wavelengths for the different monitored diffraction orders due to differing incident angles.

ethanol:water solutions and the difference spectra to pure water plotted for both polarizations in Figs. 8(a) and 8(b). For comparison, difference spectra for the specular reflection responses to ethanol:water are plotted in Figs. 8(c) and 8(d). A lack of a feasible method for obtaining a representative first-order reference spectrum dictated that the comparisons be made for relative reflection intensity differences, and thus the peaks in these plots do not correspond to the singularities, but rather relative shifts in the singularities. However, similar responses are exhibited for the zeroth- and first-order reflection intensity differences, where symmetries exist between the first- and zeroth-order orthogonal polarizations. This is again expected due to the coupling of all diffracted orders at the grating, and further supports the general nature of the GLRS theory in that a frequency-dependent response is exhibited in all diffraction orders.

The general shape of the absorbance data also agrees with the predicted theoretical response, including the position of the peak in the derivative, which is dependent upon the real part of the dielectric function of the methylene blue:water solutions. Figure 9 shows the absorbance response at the three different angles of incidence, which are chosen to yield GLRS thresholds in regions of different anomalous dispersion characteristics. The functional dependence of the peak height with concentration is seen in all three plots, with a larger extinction coefficient corresponding to a larger peak amplitude decline in the derivative. A real index modulation is occurring at the two lower angles of incidence due to the high concentrations of dye affecting the bulk index, and this is seen as a shift in the position of the singularity for high concentration of dye. This is a result of the Kramers-Kronig relationship between the real and imaginary parts of the dielectric function, which predicts large index shifts at wavelengths corresponding to shoulders of the absorption band for the highest concentration of dye.

Figure 10 displays the molar extinction coefficient's dependence on concentration of methylene blue in water. A shift in the absorbance maximum from 659 to 610 nm occurs with concentration due to a tautomeric reaction occurring at higher dye concentrations [14]. The imaginary dielectric values are tabulated for the six methylene blue concentrations at the three singularity wavelengths in Table I. These values are

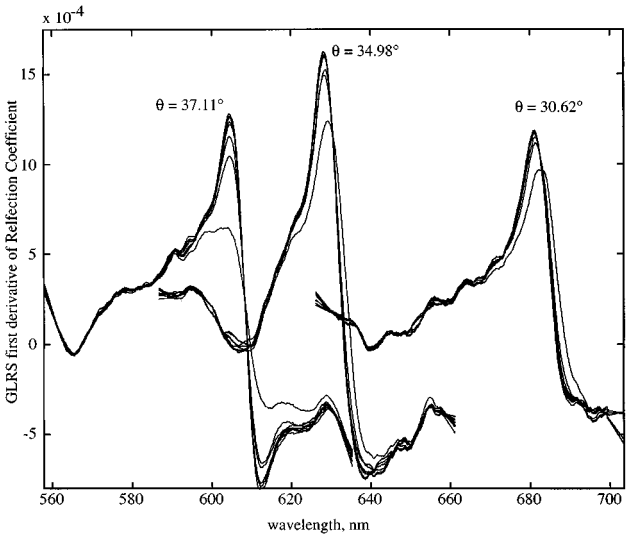

FIG. 9. GLRS derivative of relative reflection coefficients for varying concentrations of methylene blue (Aldrich, recrystallized) in deionized water: $1.000\times10^{-5}M$, $4.996\times10^{-5}M$, $1.000\times10^{-4}M$, $4.996\times10^{-4}M$, $1.022\times10^{-3}M$, and $5.127\times10^{-3}M$, p polarization incident. Increases in methylene blue concentration result in a decline in the peak amplitude that is dependent upon the imaginary part of the dielectric function [$\mathrm{Im}(\varepsilon^{(2)})$]. Three angles of incidence are shown here resulting in thresholds that occur at different wavelengths, with the positions again determined by Eq. (34).

plotted against the derivative amplitude peak modulation in Fig. 11, with water having a value of zero. The peak decline for the threshold at 605 nm follows the expected trend of a square root dependence that would be observed in the derivative of the reflection coefficients in (24). However, the peak modulations at 630 and 683 nm do not precisely follow a square root dependence on $\mathrm{Im}(\varepsilon)$. There may be a number of mechanisms affecting the peak height, including the contribution of anomalous dispersion and the nature of the tautomeric reaction, where the peak in the absorbance spectrum at

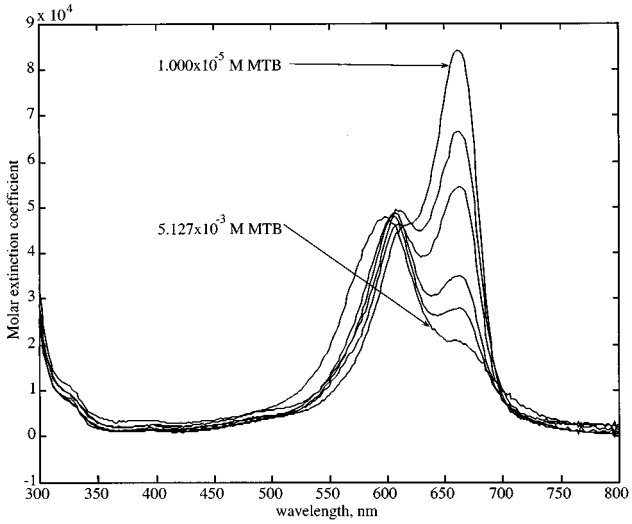

FIG. 10. Molar extinction coefficients for the six methylene blue solutions. The absorbance is nonlinear with concentration at 660 nm as the molar extinction coefficient declines with increasing concentration due to a tautomerization reaction at higher concentrations.

TABLE I. Imaginary part of the dielectric function at specific threshold wavelengths, $\mathrm{Im}(\varepsilon)=\lambda\sqrt{\mathrm{Re}(\varepsilon)}\,A_{1\ \mathrm{cm}}$, where $A_{1\ \mathrm{cm}}$ is the 1-cm pathlength absorbance of methylene blue at λ.

Methylene blue concentration (M)	$\mathrm{Im}(\varepsilon)$ at 605 nm	$\mathrm{Im}(\varepsilon)$ at 630 nm	$\mathrm{Im}(\varepsilon)$ at 683 nm
0.000 009 99	0.000 0742	0.000 0935	0.000 0970
0.000 049 96	0.000 4263	0.000 4335	0.000 4005
0.000 099 92	0.000 8055	0.000 7583	0.000 6632
0.000 4996	0.004 361	0.003 173	0.002 210
0.001 022	0.008 892	0.005 904	0.003 853
0.005 127	0.044 35	0.028 10	0.017 70

660 nm introduces a nonlinearity into the response that compensates for the nonlinear response of the GLRS derivative. In addition, the underlying grating function coupled with the modulation in $\mathrm{Re}(\varepsilon^{(2)})$ due to anomalous dispersion may affect the peak height dependence on $\mathrm{Im}(\varepsilon^{(2)})$.

V. CONCLUSIONS

The results of the theoretical and experimental study of GLRS can be formulated as follows. Near the parameter combination corresponding to the transformation of one of the diffraction orders from a traveling wave to an evanescent one all diffracted beams have singularities of the type presented in Fig. 2. The study of light reflection near these singularities at different polarizations, frequencies, and incident angles allows us to extract a rich amount of information about the studied system. It was demonstrated using GLRS that it is possible to find out the dielectric properties of the bulk, surface interface, and the grating. When interpreting results, it is very important that near the thresholds the de-

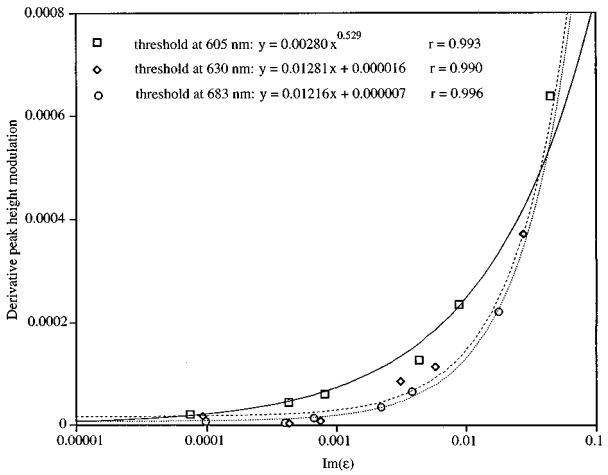

FIG. 11. GLRS derivative peak magnitude modulations for methylene blue solutions at three angles of incidence, p-polarization incident. Magnitude modulations were calculated from the baseline peak height for water and plotted vs $\mathrm{Im}(\varepsilon^{(2)})$. The response of the peak at 605 nm to increases in $\mathrm{Im}(\varepsilon^{(2)})$ follows the square root dependence predicted by the derivative of Eq. (24). Deviations from this relationship in the other two threshold positions result in a linear dependence of the peak height decline on $\mathrm{Im}(\varepsilon^{(2)})$.

pendence on bulk properties can be separated from the influence of surface properties. The contributions of both the real part of the bulk dielectric function and the imaginary part may be separated as well. The first quantity defines the position of the singularity and the second one the behavior of scattering amplitudes and phases just before and after the singularity, respectively.

The analysis of the light scattering threshold singularities can provide information on static systems as well as on dynamic processes occurring at and near the grating surface, including the influence of hydrodynamic and double-layer fluctuations, cavitation, and so on. The analysis of the effect of the scattering of evanescent light waves in the critical channel by small particles dispersed in the sample medium [15] can provide important information on the structure and dynamics of colloid systems. The characteristic optical lengths of evanescent waves have the same order of magnitude as the diffusion and hydrodynamic surface sublayers and the double layer in dilute to moderately concentrated electrolyte solutions.

In conclusion we would like to stress that the analysis of the singularities of the wave scattering from grating covered surfaces can be useful, not only in the case of light waves, but also in the cases of other types of waves: acoustic waves, microwaves, and even neutron and atomic de Broglie waves. In the last case, the high-quality physical grating may be replaced by a laser standing wave of the kind described in [16].

ACKNOWLEDGMENTS

The authors wish to thank Nanofilm, Inc. for fabrication assistance, and the Center for Process Analytical Chemistry and Security Pacific Bank for financial support of this work.

[1] X. Mai, R. Moshrefzadeh, U. J. Gibson, G. I. Stegeman, and C. T. Seaton, Appl. Spectosc. **24**, 3155 (1985).

[2] K. Tiefenthaler and W. Lukosz, J. Opt. Soc. Am. **36**, 209 (1989).

[3] N. Dushkina and S. Sainov, J. Mod. Opt. **39**, 173 (1992); S. Sainov, B. Chernov, and N. Dushkina, Opt. Lasers Eng. **18**, 297 (1993).

[4] S. M. Rytov and I. L. Fabelynskii, Zh. Eksp. Teor. Fiz. **20**, 340 (1950).

[5] B. B. Anderson, A. M. Brodsky, and L. W. Burgess, Anal. Chem. **68**, 1081 (1986).

[6] D. Hall, *Progress in Optics*, edited by E. Wolf (Elsevier, Amsterdam, 1991), Vol. 29; A. Brodsky and M. Urbach, Prog. Surf. Sci. **33**, 1 (1990).

[7] H. Raether, *Surface Plasmons of Smooth and Rough Surfaces and on Gratings* (Springer, Berlin, 1988).

[8] R. Newton, *Scattering Theory of Waves and Particles* (McGraw-Hill, New York, 1966).

[9] A. Baz' and L. Okun', Zh. Eksp Teor. Fiz. **35**, 757 (1958) [Sov. Phys. JETP **35**, 757 (1958)].

[10] We follow the theory of wave scattering in the stationary picture [8]. For the interpretation of the described effects in some cases it is more convenient to refer to nonstationary theory [8] in which, for example, $\int g(\tilde{\omega}) r_{\alpha,\alpha'}(\tilde{\omega}) d\tilde{\omega}$ has to be substituted for $r_{\alpha,\alpha'}(\omega)$ with the function $g(\tilde{\omega})$ strongly peaked near $\tilde{\omega}=\omega$. In the framework of nonstationary theory it is possible to demonstrate the characteristic threshold increase in the scattering time delay $T=d[\arg(r_{\alpha\alpha})]/d\omega \sim 1/\sqrt{\delta}$ for $\delta \to 0$.

[11] L. Landau and E. Lifshitz, *Quantum Mechanics* (Pergamon, New York, 1984), Sec. 136.

[12] The expression (25) can also be obtained by the perturbative solution of the regularized integral equations for the light surface scattering (See A. Brodsky and M. Urbach, Usp. Fiz. Nauk **138**, 413 (1982) [Sov. Phys. Usp. **25**, 810 (1982)]).

[13] L. Landau and E Lifshitz, *Electrodynamics of Continuous Media* (Pergamon, New York, 1985).

[14] H. J. Conn, *Biological Stains*, 6th ed. (Biotech Publications, Geneva, NY, 1953), p. 111.

[15] H. Chur, D. S. Wang, and M. Kerker, Appl. Opt. **18**, 2679 (1979).

[16] D. Giltner, R. McGowan, and S. Lee, Phys. Rev. A **52**, 3966 (1995).